J. Fluid Mech. (2000), *vol.* 414, *pp.* 339–366. Printed in the United Kingdom

One-dimensional nonlinear stability of pathological detonations

By GARY J. SHARPE AND S. A. E. G. FALLE
Department of Applied Mathematics, University of Leeds, Leeds LS2 9JT, UK

(Received 6 August 1999 and in revised form 27 February 2000)

In this paper we perform high-resolution one-dimensional time-dependent numerical simulations of detonations for which the underlying steady planar waves are of the pathological type. Pathological detonations are possible when there are endothermic or dissipative effects in the system. We consider a system with two consecutive irreversible reactions A→B→C, with an Arrhenius form of the reaction rates and the second reaction endothermic. The self-sustaining steady planar detonation then travels at the minimum speed, which is faster than the Chapman–Jouguet speed, and has an internal frozen sonic point at which the thermicity vanishes. The flow downstream of this sonic point is supersonic if the detonation is unsupported or subsonic if the detonation is supported, the two cases having very different detonation wave structures. We compare and contrast the long-time nonlinear behaviour of the unsupported and supported pathological detonations. We show that the stability of the supported and unsupported steady waves can be quite different, even near the stability boundary. Indeed, the unsupported detonation can easily fail while the supported wave propagates as a pulsating detonation. We also consider overdriven detonations for the system. We show that, in agreement with a linear stability analysis, the stability of the steady wave is very sensitive to the degree of overdrive near the pathological detonation speed, and that increasing the overdrive can destabilize the wave, in contrast to systems where the self-sustaining wave is the Chapman–Jouguet detonation.

1. Introduction

The governing equations for detonation waves (supersonic shock-induced combustion waves) admit solutions in which the flow is steady (in the shock frame) and one-dimensional, the so-called Zeldovich–Neumann–Döring waves (see, for example, von Neumann 1942). These waves can be self-sustaining, where the heat released by the reactions is exactly enough to continue to drive the shock. There are two possible forms for such self-sustained steady waves (Wood & Salsburg 1960). If the system in not too complex, then the self-sustaining wave is the Chapman–Jouguet (CJ) detonation, which travels at the minimum possible speed and the flow is then equilibrium sonic at the end of the reaction zone. However, complexities in the system (such as endothermic stages of the reaction, mole changes during the reaction, more than one reversible reaction, transport effects, relaxational degrees of freedom; see Fickett & Davis 1979 for examples) can cause the self-sustaining wave to be of the so-called pathological type, and then the CJ wave does not exist. Such pathological detonations travel faster than the CJ speed and the reaction zone has an internal frozen sonic point (the pathological point) at which the thermicity vanishes. The detonation has

two possible wave structures downstream of the sonic point, supersonic or subsonic, corresponding to unsupported and supported pathological detonations respectively. For instance, in astrophysics, due to an endothermic stage of the reactions, pathological detonations can occur in white dwarf stars, which are believed to be responsible for some supernovae events (Sharpe 1999*a*).

Overdriven detonations, which travel faster than the self-sustaining speed and are subsonic throughout, are also possible and correspond to piston-supported detonations.

Experiments (Fickett & Davis 1979) reveal that detonations usually have a complicated three-dimensional time-dependent structure (cellular detonations). However, in some cases the flow is principally one-dimensional, where the front oscillates longitudinally. Such galloping detonations are seen when blunt bodies are fired into reactive gases at supersonic velocities (e.g. Alpert & Toong 1972; Lehr 1972). There appear to be two types of galloping detonations, which Fickett & Davis (1979) classify as fast and slow galloping detonations. In the fast gallop the period is very regular, but for the slow gallop the period is irregular and much longer. The slow gallop is also seen (very rarely) in tubes with square cross-sections, in which the detonation fails and decomposes into a flame decoupled from the leading shock. After an induction time the detonation is re-ignited, only to fail again, and so the process is repeated (Saint-Cloud *et al.* 1972).

In these cases the steady planar wave is unstable to one-dimensional perturbations. Hence a first step in understanding such galloping detonations is a linear stability analysis. Various methods have been developed for determining the linear stability response of detonation waves (Erpenbeck 1962; Lee & Stewart 1990; Sharpe 1997). These have mostly been applied to simple systems for which the self-sustaining wave is of the CJ type (Erpenbeck 1964; Lee & Stewart 1990; Sharpe 1997; Short & Quirk 1997). However, Sharpe (1999*b*) determined the linear stability of the system used in this paper, where the self-sustaining detonation is of the pathological type due to a second reaction being endothermic. He found that the linear stability of pathological detonations was qualitatively the same as for CJ detonations. However, he also found that the stability of overdriven detonations was very sensitive to the detonation speed near the self-sustaining speed, and increasing the overdrive could destabilize the steady wave, which is very different behaviour than for systems where the self-sustaining detonation is CJ.

One-dimensional time-dependent numerical calculations for CJ detonations and their overdriven counterparts (Fickett & Wood 1966; Bourlioux, Majda & Roytburd 1991; Williams, Bauwens & Oran 1996; Short & Quirk 1997; Sharpe & Falle 1999) have shown that the linear stability analysis gives an excellent prediction for the stability boundary, and for the frequency of oscillation if the detonation is not too unstable. However, for detonations further from the stability boundary, nonlinear effects quickly become important, and irregular oscillations are observed. Both the slow and fast gallop, and the detonation failure are seen in such one-dimensional simulations.

In this paper we consider the long-time unsteady behaviour of a system where the self-sustaining detonation is of the pathological type, specifically the system considered in the linear stability analysis of Sharpe (1999*b*). In the linear approximation, no perturbations downstream of the sonic point can affect the region of the detonation between the shock and the sonic point, and hence the linear stability analysis does not take into account whether the pathological detonations is supported or unsupported. However, as suggested in Sharpe (1999*b*), since the structures of the supported and

unsupported steady pathological detonation waves are quite different downstream of the sonic point, the long time nonlinear stability of the two waves might also be very different, especially for very unstable detonations. We also investigate whether the sensitive dependence of the linear stability of overdriven detonations on the detonation speed, for speeds near the pathological speed, is seen in the nonlinear simulations.

In § 2 we give the governing equations and non-dimensionalization. The steady one-dimensional waves are then considered in § 3. The numerical method is discussed in § 4, while the results and conclusions are given in § 5 and § 6.

2. Governing equations

In this paper we use a model system with two consecutive irreversible reactions A→B→C, with Arrhenius forms of the reaction rates and the second reaction endothermic. The governing equations are, in one dimension,

$$\left.\begin{aligned} &\frac{\mathrm{D}\rho}{\mathrm{D}t}+\rho\frac{\partial u}{\partial x}=0, \quad \rho\frac{\mathrm{D}u}{\mathrm{D}t}=-\frac{\partial p}{\partial x}, \quad \frac{\mathrm{D}e}{\mathrm{D}t}+p\frac{\mathrm{D}\rho^{-1}}{\mathrm{D}t}=0,\\ &\frac{\mathrm{D}\lambda_1}{\mathrm{D}t}=\frac{W_1}{\rho}, \quad \frac{\mathrm{D}\lambda_2}{\mathrm{D}t}=\frac{W_2}{\rho}, \quad \frac{\mathrm{D}}{\mathrm{D}t}=\frac{\partial}{\partial t}+u\frac{\partial}{\partial x}, \end{aligned}\right\} \tag{2.1}$$

where u is the fluid velocity in the laboratory frame, ρ the density, p the pressure, e the internal energy per unit mass, λ_i the reaction progress variable of the ith reaction ($i = 1$ or 2, with $\lambda_i = 1$ for unburnt and $\lambda_i = 0$ for burnt), γ the (constant) ratio of specific heats and W_i the reaction rate of the ith reaction. The internal energy per unit mass is given by

$$e(\rho, p, \lambda) = \frac{p}{(\gamma-1)\rho} - Q, \tag{2.2}$$

where

$$Q = q_1(1-\lambda_1) + q_2(1-\lambda_2) \tag{2.3}$$

is the total heat release and q_i is the constant heat of reaction for the ith reaction. Note that $q_2 < 0$ since the second reaction is assumed to be endothermic. The mass fractions x_A, x_B, x_C of species A, B, C are related to the reaction progress variables by

$$\mathrm{x}_A = \lambda_1, \quad \mathrm{x}_B = \lambda_2 - \lambda_1, \quad \mathrm{x}_C = 1 - \lambda_2. \tag{2.4}$$

We assume an Arrhenius form of the reaction rates and a perfect gas:

$$W_1 = -K_1\rho\lambda_1 \mathrm{e}^{(-T_{A1}/T)}, \quad W_2 = K_2\rho(\lambda_1-\lambda_2)\mathrm{e}^{(-T_{A2}/T)}, \quad T = \frac{\mu p}{R\rho}, \quad c^2 = \frac{\gamma p}{\rho}, \tag{2.5}$$

where T is the temperature, c the sound speed, T_{Ai} the activation temperature of the ith reaction, K_i the constant rate coefficient for the ith reaction, R the universal gas constant and μ the (constant) mean molecular weight. It is also useful to define the sonic parameter

$$\eta = c^2 - u^2. \tag{2.6}$$

Henceforth we use an overbar to denote dimensional quantities, a zero (0) subscript to denote steady unperturbed quantities, an s superscript to denote quantities at a sonic point, a p superscript to denote quantities at the pathological point, an infinity (∞) superscript to denote quantities at the end of the reaction zone and a minus ($-$) subscript to denote quantities in the ambient upstream state.

We non-dimensionalize by putting

$$\left.\begin{aligned} \rho &= \frac{\bar{\rho}}{\bar{\rho}_-}, \quad \boldsymbol{v} = \frac{\bar{\boldsymbol{v}}}{\bar{D}}, \quad p = \frac{\bar{p}}{\bar{\rho}_-\bar{D}^2}, \quad T = \frac{p}{\rho} = \frac{\bar{R}\bar{T}}{\mu\bar{D}^2}, \\ t &= \frac{\bar{K}_1\bar{t}}{\alpha_1}, \quad \boldsymbol{r} = \frac{\bar{K}_1\bar{\boldsymbol{r}}}{\alpha_1\bar{D}}, \quad q_1 = \frac{\bar{q}_1}{\bar{D}^2}, \quad q_2 = \frac{\bar{q}_2}{\bar{D}^2}, \end{aligned}\right\} \tag{2.7}$$

where $\bar{D}$ is the speed of the steady detonation wave and α_1 is a scale factor chosen so that the characteristic length scale is the half-reaction length of the first reaction, i.e. the distance between the shock and the point at which $\lambda_1 = 1/2$ in the steady wave. We then define non-dimensional activation temperatures, τ_1, τ_2, by

$$\tau_1 = \frac{\bar{R}\bar{T}_{A1}}{\mu\bar{D}^2}, \quad \tau_2 = \frac{\bar{R}\bar{T}_{A2}}{\mu\bar{D}^2} \tag{2.8}$$

and the non-dimensional pressure in the ambient material by

$$p_- = \frac{\bar{p}_-}{\bar{\rho}_-\bar{D}^2}. \tag{2.9}$$

In terms of these non-dimensional variables (2.1) are unchanged in form except that the reaction rates are now given by

$$W_1 = -\alpha_1\rho\lambda_1\exp(-\tau_1\rho/p), \quad W_2 = \alpha_2\rho(\lambda_1 - \lambda_2)\exp(-\tau_2\rho/p), \tag{2.10}$$

where $\alpha_2 = \alpha_1\bar{K}_2/\bar{K}_1$. Let $\alpha = \alpha_2/\alpha_1$.

The majority of the results of previous work on the stability of detonations has been given in terms of the more familiar scalings of Erpenbeck (1964), who scaled the activation temperature and heat of reaction by the temperature in the ambient material. In terms of this scaling we define

$$E_1 = \frac{\bar{T}_{A1}}{\bar{T}_-}, \quad E_2 = \frac{\bar{T}_{A2}}{\bar{T}_-}, \quad Q_1 = \frac{\bar{q}_1\mu}{\bar{R}\bar{T}_-}, \quad Q_2 = \frac{\bar{q}_2\mu}{\bar{R}\bar{T}_-}. \tag{2.11}$$

Note that

$$\bar{T}_- = \frac{\mu\bar{p}_-}{\bar{R}\bar{\rho}_-} = \frac{\mu}{\bar{R}}\bar{D}^2 p_- \tag{2.12}$$

so that the conversion between his scalings and ours is given by

$$E_i = \frac{\tau_i}{p_-}, \quad Q_i = \frac{q_i}{p_-}. \tag{2.13}$$

Throughout this paper we set

$$\gamma = 1.2, \quad \alpha = 1, \tag{2.14}$$

and, unless otherwise specified, we use the values of the heat releases

$$Q_1 = 100, \quad Q_2 = -75. \tag{2.15}$$

Note that for $\tau_1 = \tau_2 = 0$ this reduces to the pathological detonation model of Fickett & Davis (1979).

3. Steady one-dimensional detonations

In this section we describe the steady one-dimensional detonation waves for our model. For a discussion of the qualitative nature of such solutions based on Hugoniot curves and Rayleigh lines see Fickett & Davis (1979) or Sharpe (1999*b*).

In terms of our non-dimensional variables, the steady detonation is assumed to travel at unit speed in the positive x-direction in the laboratory frame. We transform to a frame moving with the shock, i.e.

$$x = x^l - t, \quad u = u^l - 1, \tag{3.1}$$

where x^l and u^l are the position and the fluid velocity in the laboratory frame. The shock is now stationary at $x = 0$ and the detonation wave lies in the negative-x half-plane.

Conservation of mass and momentum then give

$$\rho_0 u_0 = -1, \quad p_0 + \rho_0 u_0^2 = p_- + 1, \tag{3.2}$$

which allows us to write the thermodynamic variables in terms of u_0 alone:

$$\rho_0 = -\frac{1}{u_0}, \quad p_0 = p_- + 1 + u_0. \tag{3.3}$$

The sonic value of u_0 can then be found from

$$\eta_0 = c_0^2 - u_0^2 = -\gamma(p_- + 1 + u_0)u_0 - u_0^2 = 0, \tag{3.4}$$

which gives

$$u_0^s = -\frac{\gamma(p_- + 1)}{\gamma + 1}. \tag{3.5}$$

Conservation of energy gives

$$\frac{\gamma p_0}{(\gamma - 1)\rho_0} + \frac{1}{2}u_0^2 = \frac{1}{2} + \frac{\gamma p_-}{(\gamma - 1)} + Q_0, \tag{3.6}$$

where

$$Q_0 = q_1(1 - \lambda_{10}) + q_2(1 - \lambda_{20}). \tag{3.7}$$

This gives a relation between the thermodynamic and chemical variables:

$$Q_0 = -\frac{(u_0 + 1)}{2(\gamma - 1)}\left[(\gamma + 1)u_0 + 2\gamma p_- + \gamma - 1\right] \tag{3.8}$$

or

$$\begin{aligned} u_0 &= -\frac{\gamma(p_- + 1)}{\gamma + 1} \pm \frac{\left[(1 - \gamma p_-)^2 - 2(\gamma^2 - 1)Q_0\right]^{1/2}}{\gamma + 1} \\ &= u_0^s \pm \frac{\left[2(\gamma^2 - 1)(Q_0^s - Q_0)\right]^{1/2}}{\gamma + 1}, \end{aligned} \tag{3.9}$$

so that u_0 and hence the other thermodynamic variables are double valued for a given value of the total heat release, everywhere except at a sonic point. The thermodynamic quantities therefore have a subsonic, or strong, branch corresponding to the plus sign and a supersonic, or weak, branch corresponding to the minus sign and the solution can only pass continuously from one branch to the other at a sonic point. Note that

$$\frac{\mathrm{d}Q_0}{\mathrm{d}u_0} = \frac{\eta_0}{(\gamma - 1)u_0} \tag{3.10}$$

so that

$$\frac{\mathrm{d}u_0}{\mathrm{d}x} = \frac{u_0(\gamma - 1)}{\eta_0}\frac{\mathrm{d}Q_0}{\mathrm{d}x}, \tag{3.11}$$

which diverges at a sonic point unless $\mathrm{d}Q_0/\mathrm{d}x = 0$ there, i.e. the total heat release must be a maximum there, otherwise no steady solution can exist.

At the shock $\lambda_{10} = \lambda_{20} = 1$, $Q_0 = 0$ and the flow is subsonic so that

$$u_{0+} = \frac{1 - 2\gamma p_- - \gamma}{\gamma + 1}. \tag{3.12}$$

The weak branch gives $u_0 = -1$ at $x = 0$, i.e. it corresponds to an unshocked state.

At the end of the reaction zone $\lambda_{10} = \lambda_{20} = 0$ and $Q_0 = q_1 + q_2$ which gives

$$u_0^\infty = -\frac{\gamma(p_- + 1)}{\gamma + 1} \pm \frac{\left[(1 - \gamma p_-)^2 - 2(\gamma^2 - 1)(q_1 + q_2)\right]^{1/2}}{\gamma + 1}. \tag{3.13}$$

For pathological detonations, the detonation speed, $\bar{D}^p$, cannot be determined analytically, but is an eigenvalue of the governing equations. However, although the CJ wave is forbidden when the detonation is pathological, one can still determine what the CJ speed should be. The CJ condition is that the flow is sonic for the complete reaction value of Q_0, which gives

$$q_1^{CJ} + q_2^{CJ} = \frac{(1 - \gamma p_-^{CJ})^2}{2(\gamma^2 - 1)}. \tag{3.14}$$

We define the degree of overdrive with respect to the CJ speed, f^{CJ}, by

$$f^{CJ} = \left(\frac{\bar{D}^p}{\bar{D}^{CJ}}\right)^2. \tag{3.15}$$

Then

$$p_- = \frac{p_-^{CJ}}{f^{CJ}}, \quad q_i = \frac{q_i^{CJ}}{f^{CJ}}, \quad \tau_i = \frac{\tau_i^{CJ}}{f^{CJ}} \quad (i = 1, 2). \tag{3.16}$$

For given values of E_1, E_2, Q_1 and Q_2, p_-^{CJ} can be determined from (3.14) and (2.13), and then τ_1^{CJ}, τ_2^{CJ}, q_1^{CJ} and q_2^{CJ} can be determined from (2.13). It remains to determine f^{CJ}.

For the one-dimensional steady solution, the rate equations become

$$\left.\begin{aligned} \frac{\mathrm{d}\lambda_{10}}{\mathrm{d}x} &= -\frac{\alpha_1 \lambda_{10}}{u_0} \exp\left(\tau_1/((p_- + u_0 + 1)u_0)\right), \\ \frac{\mathrm{d}\lambda_{20}}{\mathrm{d}x} &= \frac{\alpha_2(\lambda_{10} - \lambda_{20})}{u_0} \exp\left(\tau_2/((p_- + u_0 + 1)u_0)\right), \end{aligned}\right\} \tag{3.17}$$

with u_0 given by (3.9). Alternatively, we can also use λ_{10} as the independent variable, in which case we have

$$\frac{\mathrm{d}\lambda_{20}}{\mathrm{d}\lambda_{10}} = \frac{\alpha(\lambda_{20} - \lambda_{10})}{\lambda_{10}} \exp\left((\tau_2 - \tau_1)/((p_- + u_0 + 1)u_0)\right). \tag{3.18}$$

The scale factor α_1 is given by

$$\alpha_1 = \int_0^{1/2} \frac{u_0}{\lambda_{10}} \exp\left(-\tau_1/((p_- + u_0 + 1)u_0)\right) \mathrm{d}\lambda_{10}. \tag{3.19}$$

Integrating (3.19) together with (3.18) gives α_1.

Using (3.7) and (3.8) to write λ_{20} in terms of λ_{10} and u_0, we obtain

$$\frac{\mathrm{d}u_0}{\mathrm{d}\lambda_{10}} = \frac{(\gamma-1)u_0}{\eta_0\lambda_{10}}(\alpha[Q_0-(q_1+q_2)(1-\lambda_{10})] \times \exp\left((\tau_2-\tau_1)/((p_-+u_0+1)u_0)\right) - q_1\lambda_{10}), \quad (3.20)$$

with Q_0 given by (3.8).

The pathological condition is that the flow is sonic when the thermicity is zero, i.e. when $\mathrm{d}Q_0/\mathrm{d}x = 0$. Since

$$\frac{\mathrm{d}Q_0}{\mathrm{d}x} = -q_1\frac{\mathrm{d}\lambda_{10}}{\mathrm{d}x} - q_2\frac{\mathrm{d}\lambda_{20}}{\mathrm{d}x} \quad (3.21)$$

this gives the values of λ_{10} and λ_{20} at the pathological point:

$$\lambda_{10}^p = \frac{\beta[Q_0^s-(q_1+q_2)]}{q_1-\beta(q_1+q_2)}, \quad \lambda_{20}^p = \frac{(\beta q_2-q_1)\lambda_{10}^p}{\beta q_2}, \quad (3.22)$$

where

$$\beta_i = \alpha_i \exp\left(\tau_i/((p_-+u_0^s+1)u_0^s)\right), \quad \beta = \frac{\beta_2}{\beta_1}. \quad (3.23)$$

We use an iterative procedure to find the pathological detonation speed. For a trial value of f^{CJ}, we integrate (3.20) from the shock into the reaction zone. If f^{CJ} is too small then the solution terminates at a sonic point and there is no steady solution, whereas if f^{CJ} is too large the solution corresponds to an overdriven detonation, which reaches a maximum value of the heat release and then proceeds to the strong equilibrium point. We thus obtain upper and lower bounds for the pathological degree of overdrive, f^{CJ}, and we can use these to iterate using bisection to obtain f^{CJ} to any desired degree of accuracy. A check on the convergence is given by the value of λ_{10} and λ_{20} as predicted by (3.22) for the current value of f^{CJ} compared to the values at the sonic point or at the maximum of the heat release.

Once the pathological detonation speed has been found, it remains to determine the complete steady structure beyond the sonic point. It is also good practice to integrate away from sonic points. In order to do so we find asymptotic expansions for the steady variables near the pathological point on each branch of the solution and integrate either to the shock or to an equilibrium point.

Consider the branch of the solution between the shock and the pathological point. We define a new variable

$$w = \lambda_{10} - \lambda_{10}^p \quad (3.24)$$

so that w is small near the pathological point, and expand λ_{20} in terms of w as

$$\lambda_{20} = \lambda_{20}^p + l_1 w + l_2 w^2 + l_3 w^3 + \cdots, \quad (3.25)$$

where

$$l_i = \frac{1}{i!}\left(\frac{\mathrm{d}^i\lambda_{20}}{\mathrm{d}w^i}\right)^p = \frac{1}{i!}\left(\frac{\mathrm{d}^i\lambda_{20}}{\mathrm{d}\lambda_{10}^i}\right)^p \quad (3.26)$$

with $l_1 = -q_1/q_2$ since $\mathrm{d}Q_0/\mathrm{d}w = 0$ at the pathological point. Expanding (3.9) then gives

$$u_0 = u_0^s + \left(\frac{2(\gamma-1)q_2 l_2}{\gamma+1}\right)^{1/2} w + \cdots \quad (3.27)$$

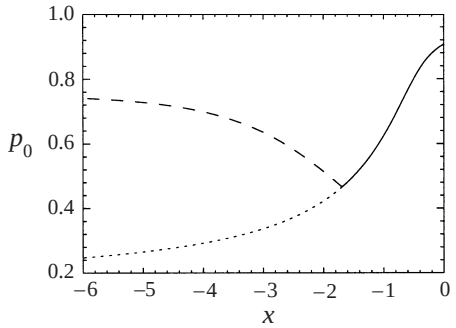

FIGURE 1. Steady pathological detonation with $E_1 = 21$, $E_2 = 20$, $Q_1 = 100$, $Q_2 = -75$, $\alpha = 1$, $\gamma = 1.2$. Pressure, p_0, versus distance behind shock, x. The solid line is the branch of the solution between the shock and the pathological point, the dotted line is the branch between the pathological point and the weak equilibrium point (corresponding to the unsupported wave) and the dashed line is the branch between the pathological point and the strong equilibrium point (corresponding to the supported wave).

so that

$$l_2 = \frac{(\gamma+1)}{2(\gamma-1)q_2}\left[\left(\frac{\mathrm{d}u_0}{\mathrm{d}w}\right)^p\right]^2. \tag{3.28}$$

Substituting into (3.18) and comparing powers of w gives the l_i. At $O(w)$ we obtain

$$\frac{(\gamma+1)}{(\gamma-1)q_2}\left[\left(\frac{\mathrm{d}u_0}{\mathrm{d}w}\right)^p\right]^2 + \frac{\gamma(\gamma-1)q_1(\tau_1-\tau_2)}{q_2(u_0^s)^3}\left(\frac{\mathrm{d}u_0}{\mathrm{d}w}\right)^p + \frac{\beta(q_1+q_2)-q_1}{q_2\lambda_{10}^p} = 0. \tag{3.29}$$

Since $\left(\mathrm{d}u_0/\mathrm{d}w\right)^p > 0$ on the branch between the shock and the pathological point, we must take the positive root.

Similarly, we can obtain asymptotic solutions in terms of w near the pathological point on the branches of the solution between the pathological point and the strong and weak equilibrium points. We can then use these asymptotic solutions as initial conditions with which to integrate (3.17) away from the sonic pathological point. Figure 1 shows the steady solution for both the supported and unsupported pathological detonations when $E_1 = 21$ and $E_2 = 20$. For these parameters, according to the linear stability analysis, the steady detonation is slightly unstable to one-dimensional disturbances. Note that for the supported pathological detonation, which goes to the strong equilibrium point, there is a discontinuity in the derivatives of the thermodynamic quantities at the pathological point. Note also that the unsupported pathological detonation takes much longer to reach equilibrium compared to the supported detonation due to the lower temperatures.

For overdriven detonations, we define the degree of overdrive by

$$f = \left(\frac{\bar{D}}{\bar{D}^p}\right)^2, \tag{3.30}$$

i.e. with respect to the pathological speed, and then the pathological detonation has $f = 1$. Figure 2 shows the steady solution for an overdriven detonation with $E_1 = 21$, $E_2 = 20$ and $f = 1.1$. For overdriven detonations the thermodynamic variables have a minimum inside the reaction zone, but their derivatives are continuous there. The structure of the supported pathological detonation is the limit of the structure of overdriven detonations as $f \to 1$ from above.

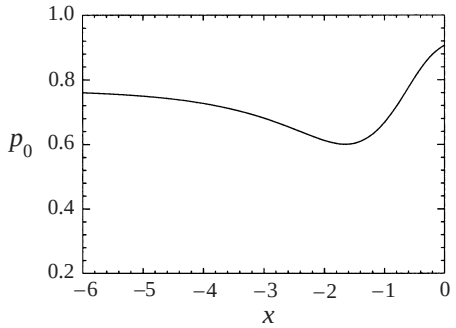

FIGURE 2. Overdriven detonation with $E_1 = 21$, $E_2 = 20$, $Q_1 = 100$, $Q_2 = -75$, $\alpha = 1$, $\gamma = 1.2$ and $f = 1.1$. Pressure, p_0, versus distance behind shock, x.

4. Numerical method

4.1. *Numerical code*

To perform the numerical simulations in this paper we use the hierarchical adaptive code, μCobra, which has been developed for industrial applications by Mantis Numerics Ltd., and is described in Falle & Giddings (1993) and Falle (1991), but for the sake of completeness it is worth summarizing its main features here. It is a second-order Godunov scheme in which the second-order Riemann problems are constructed from the primitive variables using a quadratic averaging function. An exact Riemann solver is used wherever necessary and a linear solver elsewhere. Second-order artificial dissipation is added to the fluxes determined from the Riemann solution in order to suppress the Quirk instability (Quirk 1992) and to remove the entropy oscillations behind slowly moving shocks. The form of this additional dissipation is described in Falle & Komissarov (1996). The code uses a hierarchical series of Cartesian grids $G^0, \ldots, G^N$, so that grid G^n has mesh spacing $h/2^n$, where h is the mesh spacing on the base grid G^0. Grids G^0 and G^1 cover the entire domain, but the higher grids only occupy regions where increased resolution is required.

4.2. *Initial and boundary conditions*

The initial data are determined by placing the steady solution, as determined by the methods in the previous section, on the grid with the shock initially at $x = 0$ and the detonation lying to the left. The numerical scheme introduces two perturbations. The first is due to the initial smearing of the shock over a few grid cells, while the second is due to the truncation error of the scheme. For high resolution the smearing of the shock is negligible (Short & Quirk 1997). These perturbations are sufficient to trigger the instability.

In our simulations the detonation runs from left to right in the positive x-direction. Since the fluid ahead of the detonation is in its quiescent state, this means that the right-hand boundary condition is irrelevant provided the shock remains within the domain. As discussed in Sharpe & Falle (1999), the left-hand boundary condition is somewhat more difficult. We therefore place the left boundary at least at $x = -100$, i.e. 100 half-reaction lengths behind the initial position of the front, and in all cases impose a zero-gradient condition there. As a test case to ensure this was far enough behind the front for the shock pressure histories to be independent of the rear boundary, we performed a series of calculations for the supported detonation with $E_1 = 29$ and $E_2 = 20$, where the left-hand boundary is placed at different distances

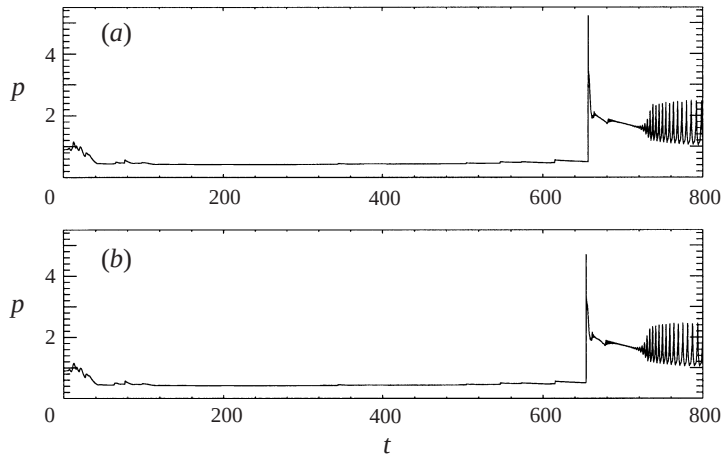

FIGURE 3. Shock pressure histories for the supported pathological detonation with $E_1 = 29$ and $E_2 = 20$ when the left-hand boundary is at (*a*) $x = -25$ and (*b*) $x = -400$.

behind the initial front. For this case the detonation quickly dies and the shock pressure drops to low values for a long time, so that the shock is moving relatively slowly and the downstream flow is very subsonic with respect to the front. Hence this constitutes a rigorous test case since waves reflected from the left-hand boundary can catch up with the front much more quickly than when the detonation is propagating at high speeds. Figure 3 shows the shock pressure histories for this case when the left-hand boundary is placed at (*a*) $x = -25$ and (*b*) at $x = -400$. The pressure history when the boundary is at $x = -100$ is also shown in figure 17(*c*). In each case the effective resolution was 256 points per half-reaction length (see § 4.3). As can be seen from the figures, the detonation quickly fails and the shock pressure remains low for a long time. However, after about $t = 650$, there is a re-ignition of the detonation and the shock pressure becomes very high. There is a small difference in the re-ignition time, strength and the subsequent flow between the cases when the left-hand boundary is at $x = -25$ and $x = -400$, indicating that the left-hand boundary can affect the flow if it is not sufficiently far to the left. However, the shock pressure histories for the cases where the left-hand boundary is at $x = -100$ and $x = -400$ are identical for the time that the calculations have been allowed to run (to $t = 800$). This shows that provided the boundary is sufficiently far to the left it has no influence on the calculation during this time, and $x = -100$ is indeed sufficiently far behind the front.

Note that for the much longer time calculations shown in figures 4 and 10 the left-hand boundary was placed at $x = -1000$.

4.3. *Resolution requirements*

μCobra controls refinement by comparing the solution of each conserved variable and also their rates of change on grids G^n and G^{n-1}. If either of these errors is greater than given tolerances then the grid is resolved to level G^{n+1}, $n + 1 \leqslant N$. These conditions can be used to ensure that regions where the flow is changing rapidly, e.g. shocks, and to some extent the reaction zone, are always resolved to the highest level. However, to ensure that the flow is always resolved wherever the reactions are fast, we resolve to the highest level whenever

$$W_i > \epsilon \tag{4.1}$$

where W_i is the reaction rate of the ith reaction ($i = 1, 2$), and ϵ is a small value. We take $\epsilon = 0.01$.

As we shall see, in some instances the detonation can fail, leading to a weak shock, followed by a long, almost reactionless, induction zone, which is in turn followed by a thin 'fire' in which the reactions take place. In these cases the induction zone tends to derefine since the flow is not changing rapidly in that region. However, small perturbations in the induction zone can produce large disturbances in the position and velocity of the fire (Buckmaster & Neves 1988), and since the size of perturbations in the induction zone is controlled by how high the resolution is there, we also ensure that the induction zone is resolved to the highest level. Indeed, we have found that there are small differences in the solutions depending on whether the induction zone is allowed to derefine or not. In order to ensure such regions are also resolved, the highest grid level is used if

$$\lambda_i > 0.1 \quad (i = 1, 2) \tag{4.2}$$

and

$$p > 2p_{-}. \tag{4.3}$$

This last condition ensures that the quiescent region ahead of the shock is not unnecessarily refined.

In this paper we use a base grid, G^0, with a mesh spacing of one point per half-reaction length of the steady detonation, and eight refinement levels, giving an effective resolution of 256 points per half-reaction length. While this may seem at first glance to be excessive, experience has shown it is necessary, especially for detonations far from the stability boundary. This is due to the fact that in the unsteady regime there can be regions where the reactions occur in a very thin region. As the detonation becomes more unstable, these regions can occur more frequently and become very much thinner. Hence the amount of resolution required to get even the qualitatively correct solution increases dramatically as the detonation becomes more unstable (Sharpe & Falle 1999). Indeed the steady wave itself tends to the 'square wave' in which the reaction take place instantaneously in a fire after a very long induction zone. Hence the number of points in the steady wave give very little indication of how many points may be required to resolve the reaction zones and heat release correctly in the unsteady regime. Secondly, such high resolution may be required to capture bifurcations in the stability behaviour correctly. For instance, we found that the position of the neutral stability boundary, as some parameter is varied, obtained from the numerical simulations depends on the resolution, but converges to exactly the value predicted by the linear stability analysis. However, at least seven refinement levels (corresponding to a resolution of 128 points per half-reaction length) were required to get the stability boundary in exact agreement with the linear stability analysis. Short & Quirk (1997) have shown for a model three-step chain-branching reaction that other bifurcations, such as period-doubling bifurcations, may require more than a 160 points per half-reaction length to capture them properly.

In order to ensure that 256 points per half-reaction length is sufficient to accurately resolve the flow for unstable detonations far from the stability boundary, a convergence study was performed for the supported detonation with $E_1 = 23$ and $E_2 = 20$. Figure 4 shows the very long-time shock pressure history for this case when the resolution is 256 points per half-reaction length (cf. figure 16). The pressure history shows that the long-time behaviour is that of a period-doubled oscillation. This calculation was repeated for resolutions of 32, 64 and 128 points per half-reaction length (or five, six and seven refinement levels, respectively). In each case the long-time solution

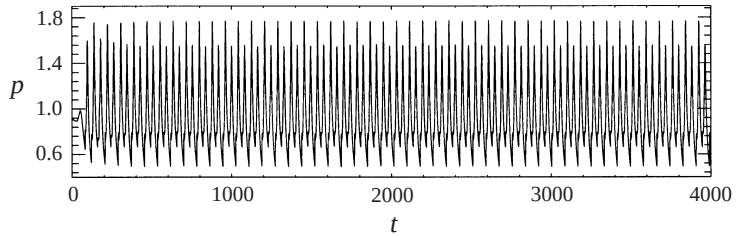

FIGURE 4. Very long-time shock pressure history for the supported pathological detonation with $E_1 = 23$, $E_2 = 20$ and a resolution of 256 points per half-reaction length.

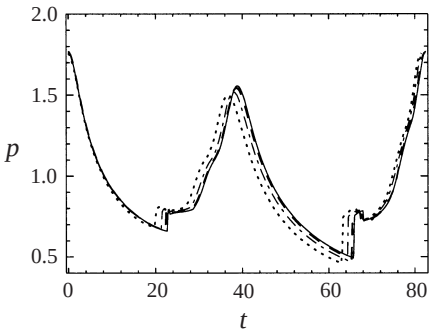

FIGURE 5. Shock pressure history through one period of the saturated oscillations for the supported pathological detonation with $E_1 = 23$, $E_2 = 20$ and resolutions of 32 (dotted line), 64 (dot-dashed line), 128 (dashed line) and 256 (solid line) points per half-reaction length.

was that of a period-doubled oscillation, but with somewhat different amplitudes and frequencies. Figure 5 shows the shock pressure histories through one saturated oscillation (i.e. between two high-amplitude peaks) for each of the four resolutions. The time scale has been shifted in each case so that the first peak occurs at $t = 0$. The two highest resolutions, corresponding to seven and eight refinement levels, are in very good agreement, and eight refinement levels are indeed sufficient to give a well-converged solution in this case. The lower resolutions give rather poor predictions for the period and amplitude of the oscillations. The final periods are 80.7, 81.6, 82.1 and 82.3 for five, six, seven and eight refinement levels respectively.

5. Results

In this section we present the results of the numerical simulations. We display plots of the pressure just behind the shock versus time as a diagnostic for the nonlinear stability. We investigate how the stability changes as various parameters are varied.

5.1. *Increasing activation temperature of first reaction*

Figure 6 shows how the pressure at the strong equilibrium point (for supported pathological detonations), at the weak equilibrium point (for the unsupported wave) and at the sonic pathological point varies with E_1 for the steady pathological detonations. Note that as the activation temperature increases the strong and weak pressure at the end of the reaction zone converge to the sonic pressure. As E_1 increases, the induction zone of the first reaction becomes much longer than for the second reaction, with the result that the delay in the second reaction over the first decreases. This has the

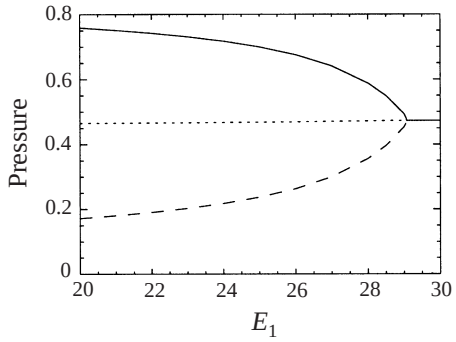

FIGURE 6. Variation of pressure at strong equilibrium point (solid line), weak equilibrium point (dashed line) and pathological point (dotted line) in the steady wave with E_1 ($E_2 = 20$).

effect that the detonation becomes less distinctly pathological, so that the sonic point moves towards the end of the reaction zone. The strong and weak values converge as the self-sustaining detonation becomes the CJ wave, when the second reaction is fast enough for the burning to remain exothermic throughout. The detonation is CJ for $E_1 > 29.067$, and there is then no difference between the supported and unsupported self-sustaining detonation waves. However, this occurs far from the stability boundary $E_1 = 20.96$. For pathological detonations away from the boundary where the wave becomes CJ, the three pressures are very distinct. The strong equilibrium pressure corresponds to the supported detonation, and hence is the pressure at the piston supporting the wave. From figure 6 it can be seen that this pressure, and thus the required piston speed, is rather high. If the detonation speed begins to decrease, the wave will quickly feel the push of the piston, and hence the speed cannot decrease too far. For the unsupported wave, however, the equilibrium pressure is low. Owing to this, and the fact that the wave is unsupported, the shock speed can fall to very low values without feeling any effects from the downstream fluid, and the detonation can fail if the shock speed becomes too low. Since the weak pressure is much less than the corresponding sonic CJ pressure, unsupported pathological detonations can die more easily than CJ detonations.

In this subsection we investigate how the stability changes for both the unsupported and supported pathological detonations as the activation temperature of the first reaction is increased. The linear stability analysis predicts that the detonation becomes more unstable as E_1 is increased, for fixed values of the other parameters (Sharpe 1999*b*). We fix the activation temperature of the second reaction to $E_2 = 20$, and then the linear stability analysis predicts stability for $E_1 < 20.96$.

Figure 7 shows the shock pressure history when $E_1 = 20.96$, for both (*a*) the unsupported detonation and (*b*) the supported pathological detonation. As mentioned in the introduction, the linear stability analysis does not take into account the flow downstream of the sonic point, and hence predicts that the stability of the unsupported and supported pathological detonation will be the same. However, except at very early times ($t < 40$) the shock pressure histories of the two cases are rather different. Both oscillate with the about the same period, 49.7 and 49.5 for the unsupported and supported waves respectively, which are in excellent agreement with the linear stability prediction of 49.7. For the unsupported detonation the shock pressure oscillates at a constant amplitude which neither grows nor decays, i.e. the steady detonation is neutrally stable, again in excellent agreement with the linear stability analysis. For the

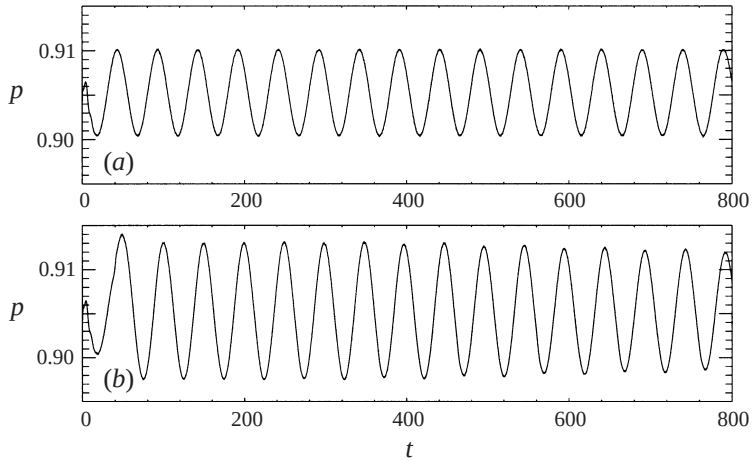

FIGURE 7. Shock pressure history for $E_1 = 20.96$ and $E_2 = 20$. (*a*) The unsupported pathological detonation and (*b*) the supported pathological detonation.

supported wave, however, the amplitude of the oscillations is much larger and is not exactly constant. There appears to be a double-mode oscillation with a low-frequency mode, not predicted by the linear stability analysis, also present. The amplitude also seems to be slightly decreasing, in which case the steady supported wave is very slightly stable, in conflict with the linear analysis.

Hence nonlinear effects seem to be important for the supported detonation, even near the stability boundary predicted by the linear analysis. Figure 8 shows profiles of the pressure, temperature and reaction progress variables for the supported detonation, at four times $t = 100.6$ (when the shock pressure is at a peak in the oscillation), $t = 112.5$, $t = 125.2$ (when the shock pressure is at a trough in the oscillation) and $t = 137.5$, during one oscillation cycle. As the pressure at the leading shock decreases, a second shock forms immediately after the internal minimum in the pressure. This is most clearly seen in the profile for $t = 125.2$. This shock remains quite weak, but increases in strength as the primary shock pressure drops, and then weakens again as the primary shock pressure increases. Note that the value of the pressure at the internal minimum also oscillates as the detonation propagates, but out of phase with the primary shock pressure (due to the fact that the particle, which is currently at the minimum pressure, was shocked at an earlier time with a different shock strength). These effects become more pronounced as E_1 is increased.

Figure 9 shows the shock pressure history for the unsupported and supported pathological detonations, when the activation temperature of the first reaction is slightly increased to $E_1 = 21$. For this value the linear stability analysis predicts that the detonation is very slightly unstable, with a single mode of period 49.7. In this case, the amplitude of the unsupported wave is slowly growing (figure 9*a*). For the supported wave however, the amplitude of the oscillation appears to quickly saturate and the double-mode oscillation is now more clearly visible. The period of the oscillation is 49.8 for the unsupported wave and 49.5 for the supported wave.

In order to check that the final amplitudes have indeed been reached for the supported case and that the double-mode instability persists, we performed a much longer calculation for this case (figure 10). It shows that the amplitudes do indeed quickly converge and the ultimate nonlinear behaviour appears to involve a period doubling with a small difference between consecutive amplitudes.

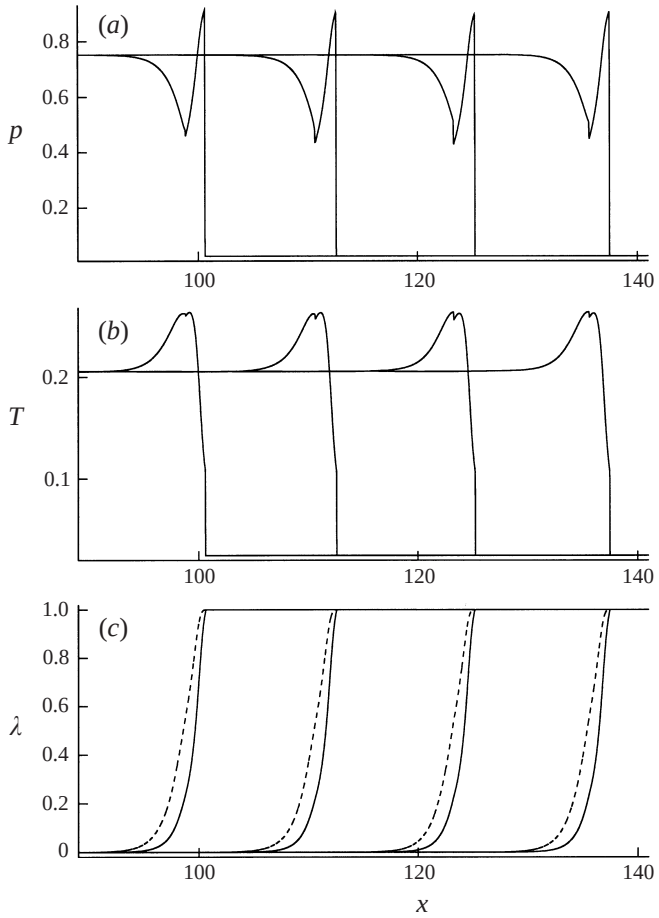

FIGURE 8. Profiles of (*a*) pressure, (*b*) temperature and (*c*) reaction progress variables, λ_1 (solid lines) and λ_2 (dashed lines), for the supported pathological detonation with $E_1 = 20.96$ and $E_2 = 20$, at times $t = 100.6$, 112.5, 125.2 and 137.5.

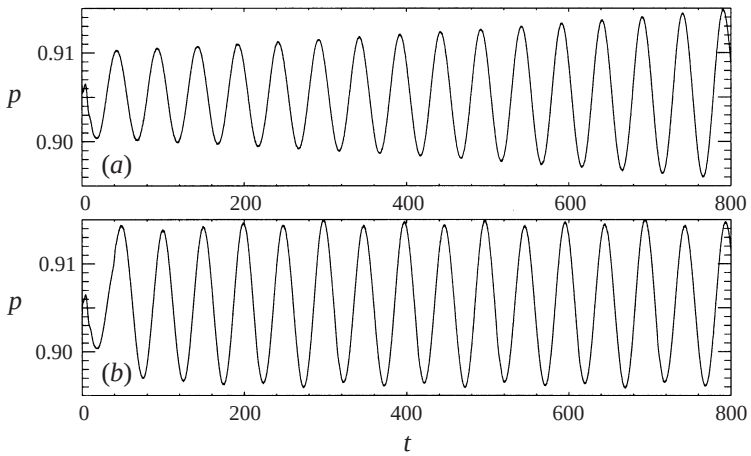

FIGURE 9. Shock pressure history for $E_1 = 21$ and $E_2 = 20$. (*a*) The unsupported pathological detonation and (*b*) the supported pathological detonation.

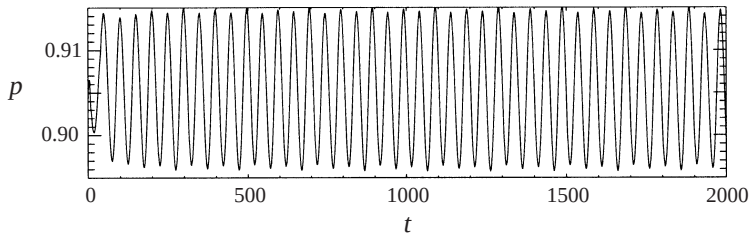

FIGURE 10. Long-time shock pressure history for the supported pathological detonation when $E_1 = 21$ and $E_2 = 20$.

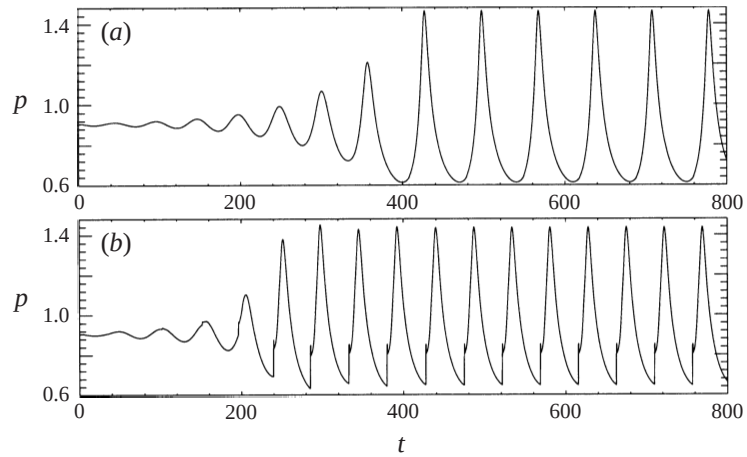

FIGURE 11. Shock pressure history for $E_1 = 21.5$ and $E_2 = 20$. (*a*) The unsupported pathological detonation and (*b*) the supported pathological detonation.

Figure 11 shows the shock pressure histories when $E_1 = 21.5$. In this case the shock pressure histories for the unsupported and the supported waves both have regular oscillations, with growing amplitudes that eventually saturate. However, the period of the oscillation is different for the two cases. The oscillations for the unsupported wave have a period of 70.2, those of the supported wave have a shorter period of 47.1, while the linear stability analysis predicts a period of 50.8. In this case, then, the period of the supported wave is in much better agreement with the linear stability analysis than that of the unsupported wave. However, this agreement would appear to be fortuitous since significant nonlinear affects are present in the supported wave. Figure 12 shows pressure profiles through one saturated oscillation for the supported wave. Note that the shock pressure is at a maximum in the oscillation at $t = 392.2$ (figure 12*a*) and at a minimum at $t = 426.0$ (figure 12*d*). As the shock pressure drops from high values, a secondary shock again forms behind the internal minimum in the pressure (figure 12*b*). The primary shock pressure continues to drop, however, so that the secondary shock begins to catch up with it (figure 12*c*). In figure 12(*d*) the secondary shock is just about to overtake the primary shock. This merging of the two shocks is responsible for the discontinuous jumps at the troughs in the shock oscillations seen in figure 11(*b*). The resulting strengthened primary shock continues to grow in strength due to a compression wave (figures 12*e* and 12*f*), until the shock pressure once again reaches a maximum, is weakened by a rarefaction, and the whole process repeats.

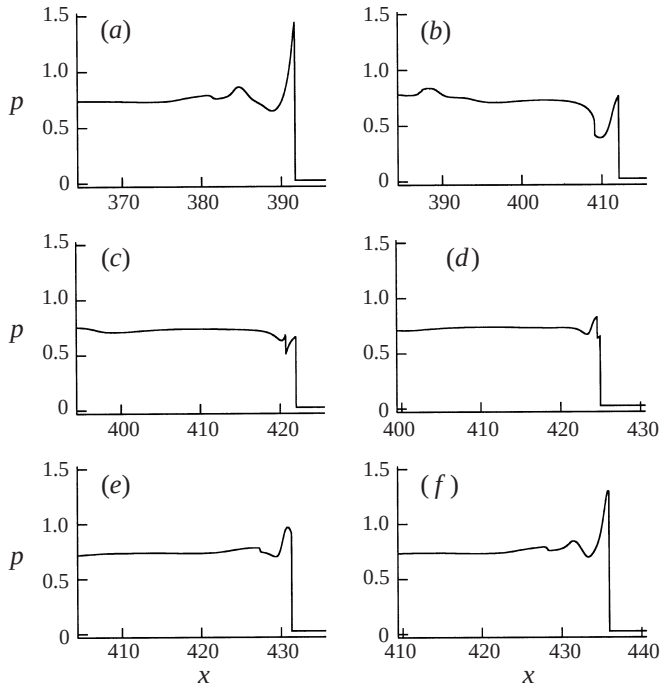

FIGURE 12. Pressure profiles for the supported pathological detonation with $E_1 = 21.5$ and $E_2 = 20$, at times (*a*) $t = 392.2$, (*b*) $t = 411.4$, (*c*) $t = 422.5$, (*d*) $t = 426.0$, (*e*) $t = 432.8$ and (*f*) $t = 437.0$.

For the steady waves, the unsupported and supported pathological detonations are distinguished by the sonic nature of the downstream flow with respect to the front (supersonic for unsupported waves and subsonic for supported waves). We now investigate how the sonic nature of the flow changes for the pulsating waves. Given the shock pressure, p_+, we can determine the instantaneous detonation speed from the equation for the jump in pressure across a shock:

$$\frac{p_+}{p_-} = 1 + \frac{2\gamma}{\gamma + 1}\left(\frac{D^2}{\gamma p_-} - 1\right).$$

This gives

$$D = \left(\gamma p_- \left[1 + \frac{\gamma + 1}{2\gamma}\left(\frac{p_+}{p_-} - 1\right)\right]\right)^{1/2}.$$

We then define the Mach number of the flow with respect to the instantaneous shock rest frame by

$$M = \frac{(D - u)}{c}.$$

In regions where $M > 1$ the flow is supersonic with respect to the front, and information from these regions moves away from the shock, whereas for $M < 1$ the flow is subsonic in the instantaneous shock rest frame and waves can catch up with the front.

Figure 13 shows the profiles of the shock-attached Mach numbers at six times, through one saturated oscillation of the unsupported wave when $E_1 = 21.5$, together with profiles of the pressure. The shock pressure is at a crest in the oscillations at

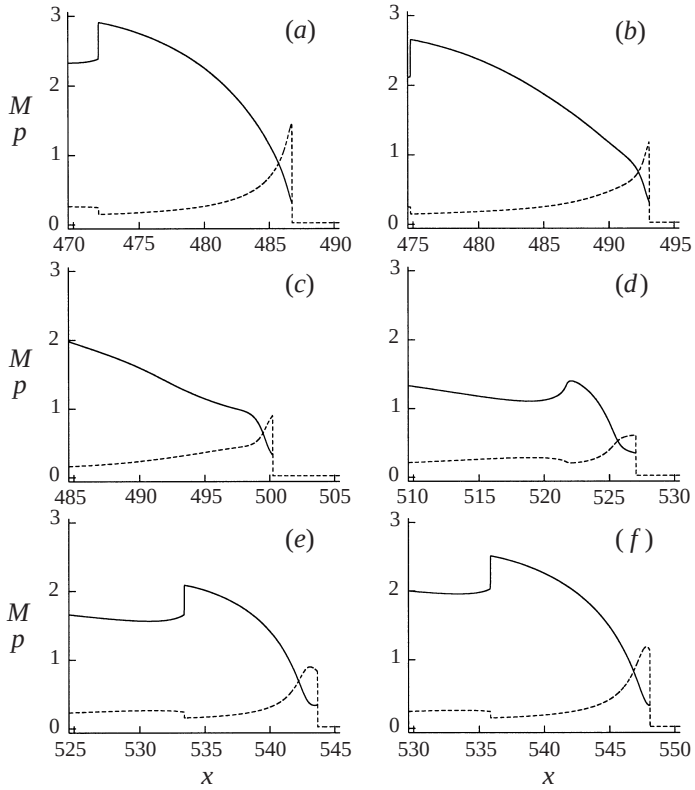

FIGURE 13. Profiles of post-shock Mach numbers in the instantaneous shock rest frame (solid lines) and pressure (dashed lines) for the unsupported pathological detonation with $E_1 = 21.5$ and $E_2 = 20$, at times (*a*) $t = 497.4$, (*b*) $t = 502.6$, (*c*) $t = 509.3$, (*d*) $t = 539.9$, (*e*) $t = 559.3$ and (*f*) $t = 563.6$.

$t = 497.4$ (figure 13*a*) and at a trough at $t = 539.9$ (figure 13*d*). Even when the shock pressure and speed are at a minimum, only a portion of the reaction zone is subsonic with respect to the front and the downstream flow is at all times supersonic. When the shock pressure is near its maximum value, and the front is moving very rapidly, the flow becomes highly supersonic with respect to the front. Hence for the unsupported pulsating wave the downstream flow can never affect the front, just as in the steady case. Note that each oscillation produces a compression wave which strengthens into a weak shock, but these weak shocks fall further and further behind the primary shock due to the supersonic nature of the flow in the regions where they form.

Figure 14 shows the profiles of the shock-attached Mach numbers at six times, through one saturated oscillation of the supported wave when $E_1 = 21.5$. When the shock pressure and speed are very near their maximum in the oscillation, the downstream flow is now slightly supersonic with respect to the front (figure 14*a*), and only the front portion of the reaction zone can affect the front. As the shock speed drops, the downstream flow becomes subsonic. However, the maximum Mach number, which occurs at the internal minimum of the pressure, can remain greater than 1, and there exists a region around the minimum pressure where the flow remains supersonic (figure 14*b*), so that the downstream flow can still not affect the front. As the shock pressure and speed fall further, the maximum Mach num-

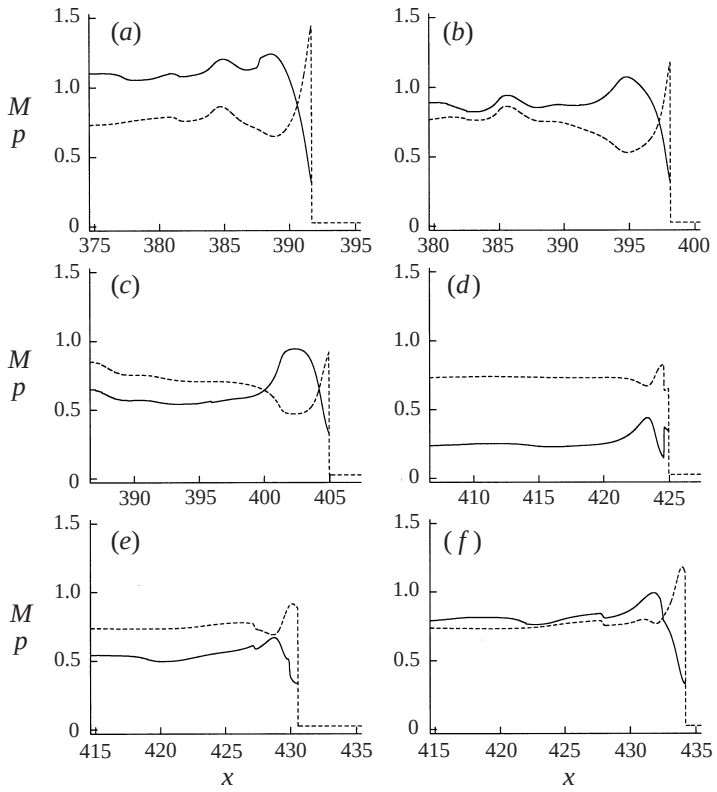

FIGURE 14. As figure 13 but for the supported pathological detonation at times (*a*) $t = 392.2$, (*b*) $t = 397.5$, (*c*) $t = 403.9$, (*d*) $t = 426.0$, (*e*) $t = 432.0$ and (*f*) $t = 435.5$.

ber drops below 1 and the entire flow becomes subsonic with respect to the front (figure 14*c*), and the flow becomes more and more subsonic as the shock speed drops even further. Now a compression wave, which forms behind the minimum in the pressure and strengthens into a weak shock, accelerates towards the primary shock due to the highly subsonic nature of the flow. The secondary shock eventually overtakes the front. (figure 14*d*), and the shock pressure and speed begin to increase again. This results in the downstream flow becoming less subsonic with respect to the front and eventually regions of the flow become supersonic again. Note that, unlike the steady supported pathological detonation where the gradient of the pressure has a discontinuity at the minimum in the pressure, for the pulsating supported wave the pressure profile is smooth at the internal pressure minimum. This is due to the fact that such discontinuities in the thermodynamic gradients move along characteristics (e.g. Fickett & Davis 1979), and once the wave becomes unstable and the minimum in the pressure is no longer sonic with respect to the front, the gradient discontinuity moves relative to the front and the pressure minimum.

The shock pressure history for $E_1 = 22$ is shown in figure 15. For this activation temperature, the unsupported wave now dies to low pressures after a large-amplitude oscillation. The shock and the reaction zone become decoupled as the shock pressure drops to low values. This failure of the detonation is also seen for CJ detonations at large activation temperatures (Short & Quirk 1997; Sharpe & Falle 1999). However,

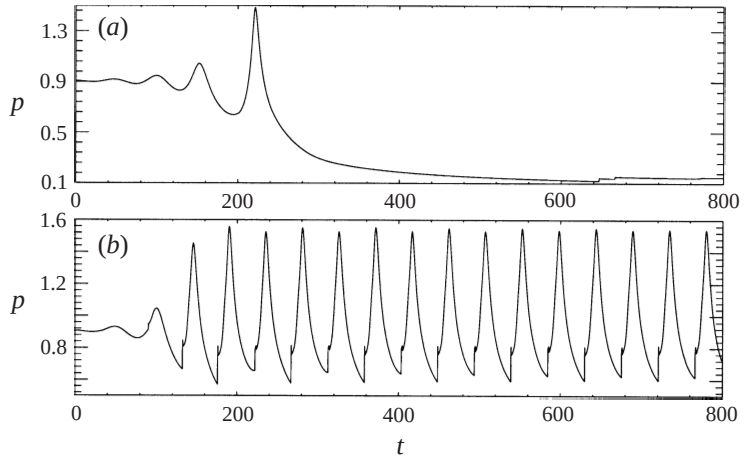

FIGURE 15. Shock pressure history for $E_1 = 22$ and $E_2 = 20$. (*a*) The unsupported pathological detonation and (*b*) the supported pathological detonation.

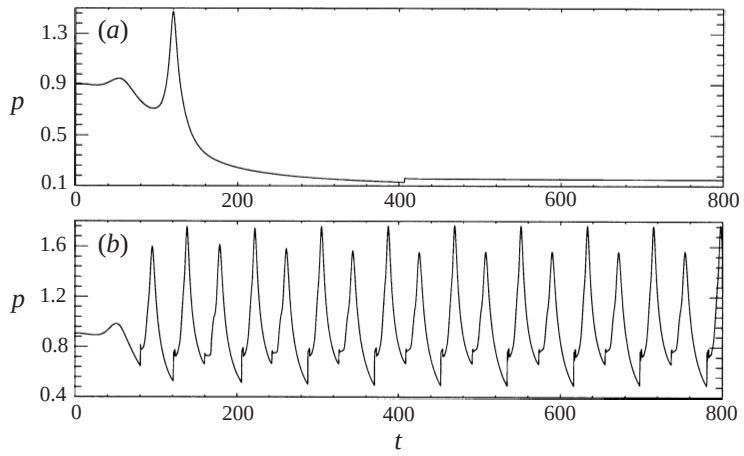

FIGURE 16. Shock pressure history for $E_1 = 23$ and $E_2 = 20$. (*a*) The unsupported pathological detonation and (*b*) the supported pathological detonation.

the supported wave still has an oscillatory behaviour, with a very regular period of 45.4, so that the stability of the unsupported wave and supported wave are very different in this case. The linear mode predicts a period of 52.5.

Figure 16 shows the shock pressure history when the activation temperature is increased to $E_1 = 23$. Now a large-amplitude oscillation followed by detonation failure occur earlier for the unsupported wave, than for $E_1 = 22$. The shock pressure history for the supported detonation is still, however, oscillatory, but there is now a clear period-doubling. The period between two crests or troughs of the same amplitude is 82.3. There is still a single linear mode with a period of 57.9.

As E_1 is increased further, the strong equilibrium pressure, and hence the piston support, begins to drop (figure 6), until the steady detonation becomes CJ at $E_1 = 29.067$. Hence as the support decreases, the supported wave will also be liable to fail. Figure 17 shows the shock pressure histories for the supported detonation when $E_1 = 25$, 27 and 29. Note that in these cases an unstable high-frequency mode can

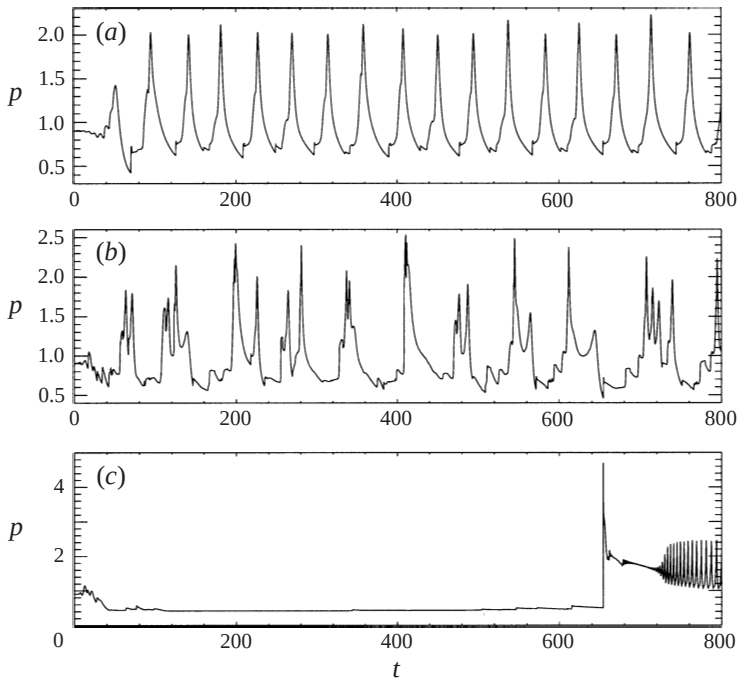

FIGURE 17. Shock pressure histories for supported pathological detonations with (*a*) $E_1 = 25$, (*b*) $E_1 = 27$ and (*c*) $E_1 = 29$ ($E_2 = 20$).

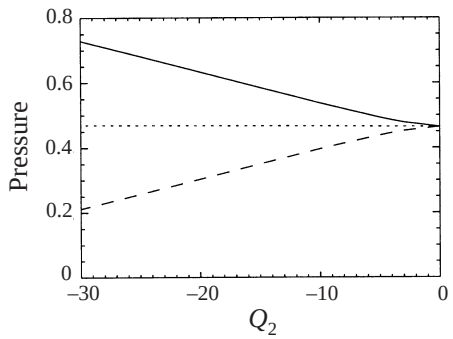

FIGURE 18. Variation of pressure at strong equilibrium point (solid line), weak equilibrium point (dashed line) and pathological point (dotted line) in the steady wave with Q_2 ($Q_1 = 50$, $E_1 = 25.26$ and $E_2 = 30$).

be seen at early times, and this becomes more unstable as E_1 increases. The linear stability analysis predicts that this mode becomes unstable at $E_1 = 24.23$. As E_1 increases it can be seen that the shock oscillations are becoming more irregular and for $E_1 = 29$ the detonation does indeed fail. However, at $t = 654.1$ the detonation re-ignites, due to a large 'explosion within the explosion' which produces a very large shock pressure. For supported waves, the failed detonation must at some point be re-ignited since the piston is constantly adding energy into the system. After the explosion the shock pressure quickly dies, but then begins to oscillate with a very short period of about 6, with a growing amplitude.

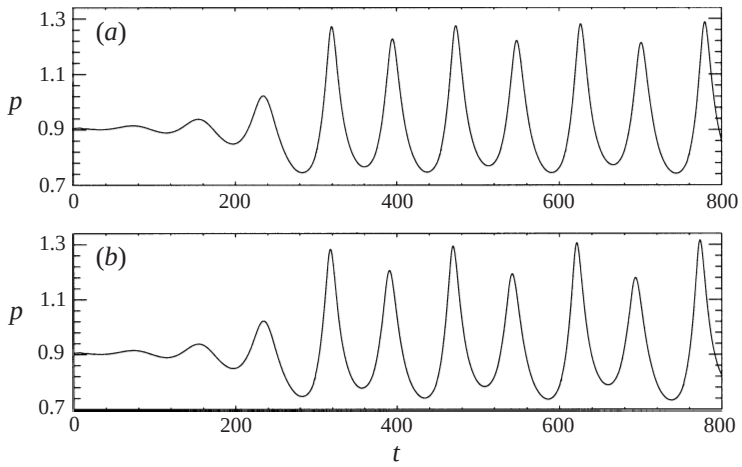

FIGURE 19. Shock pressure history for $Q_2 = -5$ ($Q_1 = 50$, $E_1 = 25.26$ and $E_2 = 30$). (a) The unsupported pathological detonation and (b) the supported pathological detonation.

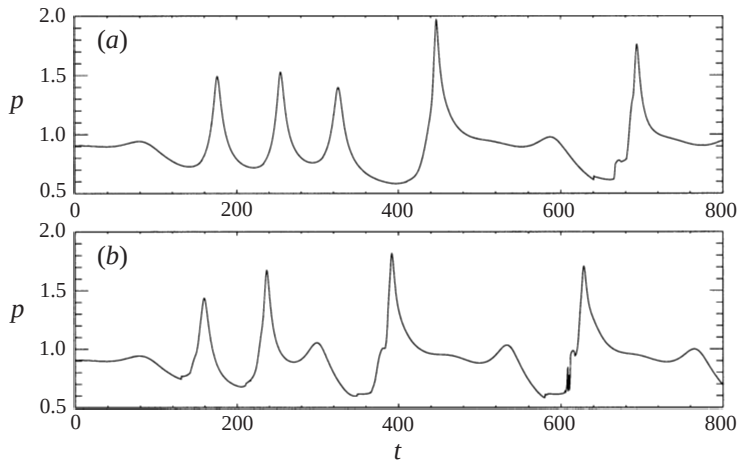

FIGURE 20. Shock pressure history for $Q_2 = -10$ ($Q_1 = 50$, $E_1 = 25.26$ and $E_2 = 30$). (a) The unsupported pathological detonation and (b) the supported pathological detonation.

5.2. *Increasing endothermicity*

In § 5.1, the steady detonation was distinctly pathological even near the stability boundary, with large differences in the downstream states for the unsupported and supported waves. As the detonations became more unstable (as E_1 was increased) the detonation became less distinctly pathological, and eventually the steady wave becomes CJ. In this subsection we consider two questions. First, how does the differences in the nonlinear stability of the unsupported and supported waves change as the steady detonations changes from being CJ, where there is no difference in the unsupported and supported waves, to pathological? Secondly, how does the stability of the two waves change if the detonation becomes more distinctly pathological as it becomes more unstable, in contrast to the previous case?

In order to accomplish this, we systematically change the heat of reaction of the second reaction, Q_2, while keeping the other parameters fixed. Clearly, for $Q_2 = 0$ there

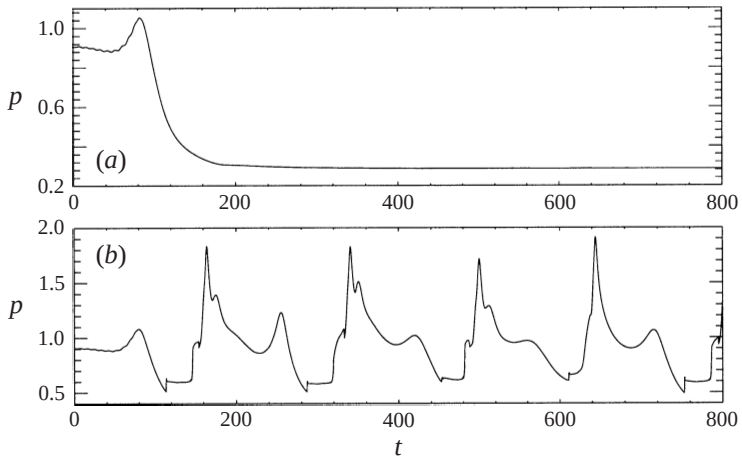

FIGURE 21. Shock pressure history for $Q_2 = -15$ ($Q_1 = 50$, $E_1 = 25.26$ and $E_2 = 30$). (*a*) The unsupported pathological detonation and (*b*) the supported pathological detonation.

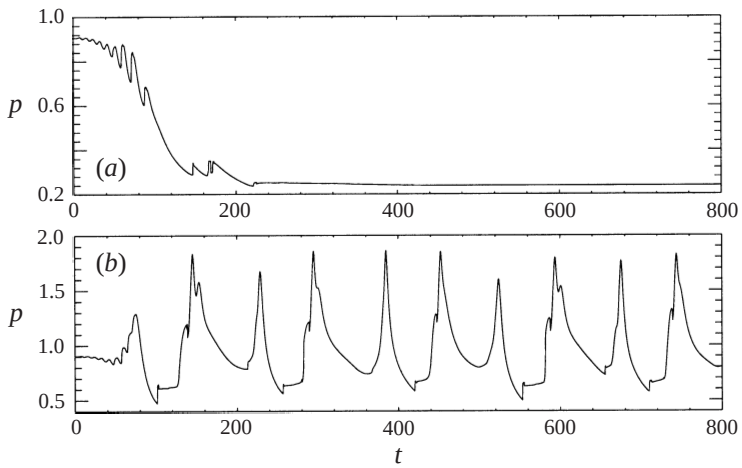

FIGURE 22. Shock pressure history for $Q_2 = -20$ ($Q_1 = 50$, $E_1 = 25.26$ and $E_2 = 30$). (*a*) The unsupported pathological detonation and (*b*) the supported pathological detonation.

is no endothermic stage and hence the steady detonation is CJ, but for increasing $|Q_2|$, the endothermic stage becomes more pronounced and hence the detonation becomes more distinctly pathological. Secondly, the linear stability analysis (Sharpe 1999*b*) shows that increasing the degree of endothermicity makes the detonation more unstable. Here we set $Q_1 = 50$ and then we choose $E_1 = 25.26$ so that the CJ detonation with $Q_2 = 0$ is neutrally stable (Sharpe 1997). We set $E_2 = 30$.

Figure 18 shows how the pressure at the strong and weak equilibrium points and at the sonic point varies with Q_2. For $Q_2 = 0$ the self-sustaining steady wave is CJ, so that the three pressures are the same there. As the degree of endothermicity increases and hence the difference between the maximum and final values of the heat release in the wave increases, the strong and weak pressures diverge. For smaller values of $|Q_2|$ there is little difference in the strong and weak equilibrium pressures and hence we expect only a small difference in the nonlinear evolution of the supported and unsupported waves. Since as $|Q_2|$ increases so does the difference in the downstream

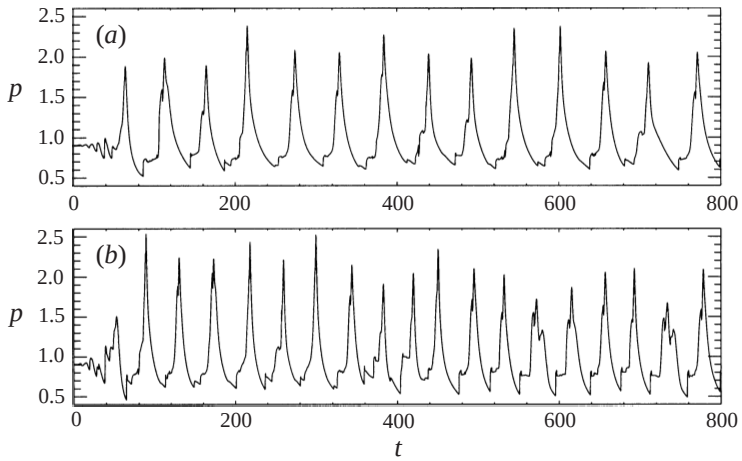

FIGURE 23. Shock pressure histories for supported pathological detonations with (*a*) $Q_2 = -30$ and (*b*) $Q_2 = -40$ ($Q_1 = 50$, $E_1 = 25.26$ and $E_2 = 30$).

pressures, we expect the differences in the nonlinear stability of the two waves to become more pronounced.

Figure 19 shows the shock pressure histories when $Q_2 = -5$. For this case there is little difference in the equilibrium pressures of the unsupported and supported steady detonations. From figure 19, it can be seen that the nonlinear stability of the two waves also is very similar, apart from small differences in the peak shock pressures. The pressure histories indicate a period-doubled oscillation with a period of 151.9 (i.e. the time between two consecutive high/low amplitude crests or troughs). For these parameters the linear stability analysis predicts a single mode with period 81.1.

The shock pressure histories for $Q_2 = -10$ are shown in figure 20. For both the unsupported and supported waves, the oscillations are now very irregular. The histories for the two cases are still qualitatively similar, but with larger differences in the values and positions of the peaks and troughs in the oscillations. These differences could lead to very different shock pressure histories for the two waves at very large times. The linear stability analysis now predicts a period of 85.6.

Figures 21 and 22 show the shock pressure histories for $Q_2 = -15$ and $Q_2 = -20$. In these cases the unsupported wave fails, while the supported detonation continues to propagate, again due to the secondary shock wave formed in the endothermic stage overtaking the dying primary shock and re-igniting the detonation. The fundamental linear mode has a period of 93.3 and 106.1 for $Q_2 = -15$ and -20 respectively. Note also that a high frequency becomes unstable, which can be seen at early times in the figures. The linear analysis predicts that this mode becomes unstable below $Q = -14.2$ and the predicted period is 8.5 for $Q = -15$ and 8.3 for $Q = -20$.

Although the detonation is becoming more unstable as the degree of endothermicity increases, the oscillation for the supported wave is actually becoming more regular with a shorter period. This is due to the effect of the increasing downstream pressure and velocity, and hence piston support (figure 18) with increasing $|Q_2|$. Figure 23 shows the histories for the supported waves when $Q_2 = -30$ and $Q_2 = -40$. In these cases the shock pressure oscillates with a nearly constant period. However, the amplitudes are quite irregular, and it appears that a very low-frequency mode is also present. Note that the high-frequency mode is now very unstable, and seems

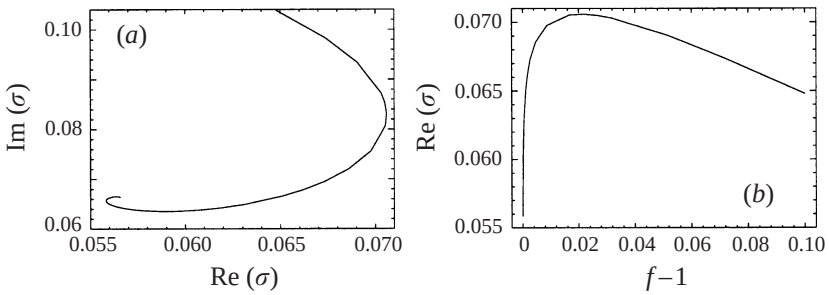

FIGURE 24. Migration of the fundamental linear mode as the degree of overdrive is varied when $E_1 = 35$, $E_2 = 50$. (*a*) Frequency versus growth rate, (*b*) growth rate versus $f - 1$ (Sharpe 1999*b*).

to be occasionally making its presence felt, even at late times. Hence in the case of increasing the degree of endothermicity, the supported detonation cannot die, no matter how unstable it is.

5.3. *Increasing degree of overdrive*

We now consider overdriven detonations, i.e. piston-supported detonations with $f > 1$. According to the linear stability analysis (Sharpe 1999*b*), the linear response to one-dimensional perturbation is very sensitive to the degree of overdrive near $f = 1$, and increasing the overdrive can actually make the detonation more unstable. This is in contrast to systems where the self-sustaining steady wave is of the CJ type, when the linear spectrum is not especially sensitive to the degree of overdrive near the CJ speed, and increasing the overdrive always makes the detonation more stable (Lee & Stewart 1990). For instance, figure 24 (taken from Sharpe 1999*b*) shows the change in the fundamental (lowest frequency) linear mode as f is varied, when $E_1 = 35$ and $E_2 = 50$. Here $\mathrm{Re}(\sigma)$ is the growth rate and $\mathrm{Im}(\sigma)$ the frequency of the disturbance. From figure 24, it can be seen that, according to the linear stability analysis, increasing the overdrive from the pathological speed has the effect of alternately stabilizing, i.e. decreasing the growth rate, destabilizing, i.e. increasing the growth rate, and then stabilizing the steady detonation wave to one-dimensional disturbances. The detonation is stable at high enough overdrive.

We now investigate how increasing the overdrive affects the stability in the nonlinear simulations. Here we take $E_1 = 20.96$ and $E_2 = 20$, so that the pathological wave is linearly neutrally stable (cf. figure 7), and hence the effect on the stability of the wave will be most clearly shown. Figure 25 shows the shock pressure histories for overdriven detonations with $f = 1.00001$, 1.0001, 1.001, 1.01, 1.1 and 1.2. It can be seen immediately from this figure that the detonation stability is very sensitive to the degree of overdrive near $f = 1$, in agreement with the linear stability analysis. Secondly, from figures 25(*a*) and 25(*b*), it can be seen that for very small increases of the overdrive the detonation is stable, while further increases make the detonation unstable again (figures 25*d*, 25*e*). For large enough overdrive, however, the detonation is stable (figure 25*f*). The shock pressure history for $f = 1.001$ (figure 25*c*) is rather peculiar. This value of the overdrive is near a stability boundary: the detonation is stable at lower overdrives and unstable at higher overdrives. However, instead of having a neutrally stable profile, like that in figure 7, there appear to be competing stabilizing and destabilizing effects.

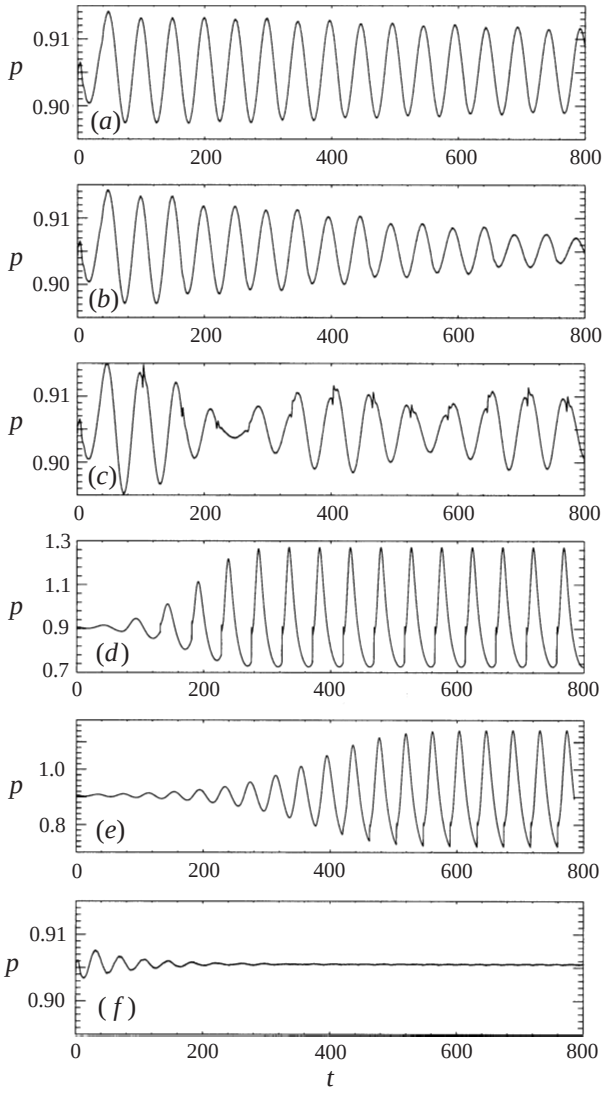

FIGURE 25. Shock pressure history for overdriven detonations with (*a*) $f = 1.00001$, (*b*) $f = 1.0001$, (*c*) $f = 1.001$, (*d*) $f = 1.01$, (*e*) $f = 1.1$ and (*f*) $f = 1.2$ ($E_1 = 20.96$ and $E_2 = 20$).

6. Conclusions

In this paper we have performed one-dimensional time-dependent calculations of pathological detonations in order to determine the nonlinear stability of such waves. We have shown that, provided the differences in the downstream states are not too small, the nonlinear evolution of the unsupported and supported pathological detonations, for fixed parameters, can be very different, even near stability boundaries. The unsupported wave can easily die, due to the downstream fluid having little effect on the detonation front. This is compounded by the endothermic stage of burning becoming subsonic with respect to the shock as it weakens and slows down, and thus withdrawing further support from the detonation front. In these cases, however, the supported detonation can remain oscillatory, with a regular or irregular period. Indeed, supported detonations have a coupled double instability, due to the instability of the

primary shock and also the formation of a secondary shock in the endothermic stage of burning, which strengthens and weakens. This secondary shock can overtake and strengthen the primary shock and re-ignite the detonation before it dies completely.

Secondly, we have shown, in agreement with the predictions of the linear stability analysis, that the stability of supported detonations is very sensitive to the detonation speed near the self-sustaining pathological speed, and that increasing the overdrive can make the detonation more unstable.

It would be perhaps more interesting to perform two-dimensional numerical simulations of such pathological waves in order to study the cellular detonation instability. The one-dimensional simulations performed in this paper suggest that the two-dimensional stability properties of unsupported and supported pathological detonations may be quite different to one another. In particular, the size and regularity of the cells could be very different. Indeed, a multi-dimensional linear stability analysis suggests that the cell size is very sensitive to the degree of overdrive (Sharpe 1999*b*). Unfortunately, the large amount of resolution required to remove the dependence of the numerically calculated cell size on the mesh spacing, combined with the very large natural cell sizes (usually between one and two orders of magnitude greater than the steady one-dimensional reaction length) and the very large space and time scales over which the detonation settles into the natural cell size configuration, make such calculations prohibitive.

G.J.S. was supported by PPARC during the course of this work.

REFERENCES

Alpert, R. L. & Toong, T.-Y. 1972 Periodicity in exothermic hypersonic flows about blunt projectiles. *Astron. Acta.* **17**, 539–560.

Bourlioux, A., Majda, A. J. & Roytburd, V. 1991 Theoretical and numerical structure for unstable one-dimensional detonations. *SIAM J. Appl. Maths* **51**, 303–343.

Buckmaster, J. & Neves, J. 1988 One-dimensional detonation stability: The spectrum for infinite activation energy. *Phys. Fluids* **31**, 3571–3576.

Erpenbeck, J. J. 1962 Stability of steady-state equilibrium detonations. *Phys. Fluids* **5**, 604–614.

Erpenbeck, J. J. 1964 Stability of idealized one-reaction detonations. *Phys. Fluids* **7**, 684–696.

Falle, S. A. E. G. 1991 Self-similar jets. *Mon. Not. R. Astron. Soc.* **250**, 581–596.

Falle, S. A. E. G. & Giddings, J. R. 1993 Body capturing. In *Numerical Methods for Fluid Dynamics* (ed. K. W. Morton & M. J. Baines), vol. 4, pp. 337–343. Clarendon.

Falle, S. A. E. G. & Komissarov, S. S. 1996 An upwind scheme for relativistic hydrodynamics with a general equation of state. *Mon. Not. R. Astron. Soc.* **278**, 586–602.

Fickett, W. & Davis, W. C. 1979 *Detonation.* University of California Press.

Fickett, W. & Wood, W. W. 1966 Flow calculations for pulsating one-dimensional detonations. *Phys. Fluids* **9**, 903–916.

Lee, H. I. & Stewart, D. S. 1990 Calculation of linear detonation stability: one-dimensional instability of plane detonation. *J. Fluid. Mech.* **216**, 103–132.

Lehr, H. F. 1972 Experiments on shock-induced combustion. *Astron. Acta.* **17**, 589–597.

Neumann, J. von 1942 In *John von Neumann, Collected Works* (ed. A. H. Taub), vol. 6. chap. 20, pp. 203–218. Pergamon.

Quirk, J. J. 1992 A contribution to the great Riemann solver debate. *ICASE Rep.* 92–64.

Saint-Cloud, J. P., Guerraud, C., Brochet, C. & Manson, N. 1972 Some properties of very unstable detonations in gaseous mixtures. *Astron. Acta.* **17**, 487–498.

Sharpe, G. J. 1997 Linear stability of idealized detonations. *Proc. R. Soc. Lond.* A **453**, 2603–2625.

Sharpe, G. J. 1999*a* The structure of steady detonation waves in type Ia supernovae: pathological detonations in C-O cores. *Mon. Not. R. Astron. Soc.* **310**, 1039–1052.

Sharpe, G. J. 1999*b* Linear stability of pathological detonations. *J. Fluid Mech.* **401**, 311–338.

Sharpe, G. J. & Falle, S. A. E. G. 1999 One-dimensional numerical simulations of idealized detonations. *Proc. R. Soc. Lond.* A **455**, 1203–1214.

Short, M. & Quirk, J. J. 1997 On the nonlinear stability and detonability limit of a detonation wave for a model three-step chain-branching reaction. *J. Fluid Mech.* **339**, 89–119.

Williams, D. N., Bauwens, L. & Oran, E. S. 1996 A numerical study of the mechanisms of self-reignition in low-overdrive detonations. *Shock Waves* **6**, 93–110.

Wood, W. W. & Salsburg, Z. W. 1960 Analysis of steady-state supported one-dimensional detonations and shocks. *Phys. Fluids* **4**, 549–566.